

Green Pea Galaxies Reveal Secrets of Ly α Escape

Huan Yang^{1,2}, Sangeeta Malhotra², Max Grönke³, James E. Rhoads², Anne Jaskot⁴,
Zhenya Zheng^{5,6}, & Mark Dijkstra³

Received _____; accepted _____

arXiv:1506.02885v1 [astro-ph.GA] 9 Jun 2015

¹CAS Key Laboratory for Research in Galaxies and Cosmology, Department of Astronomy, University of Science and Technology of China; yanghuan@mail.ustc.edu.cn

²Arizona State University, School of Earth and Space Exploration; huan.y@asu.edu; Sangeeta.Malhotra@asu.edu; James.Rhoads@asu.edu

³Institute of Theoretical Astrophysics, University of Oslo, Norway

⁴Smith College, Northampton, MA

⁵Pontificia Universidad Católica de Chile, Santiago, Chile

⁶Chinese Academy of Sciences South America Center for Astronomy, Santiago, Chile

ABSTRACT

Star-formation in galaxies generates a lot of Ly α photons. Understanding the escape of Ly α photons from galaxies is a key issue in studying high redshift galaxies and probing cosmic reionization with Ly α . To understand Ly α escape, it is valuable to study analogs of high redshift Ly α emitters in nearby universe. However, most nearby analogs have too small a Ly α equivalent width and escape fraction compared to high redshift Ly α emitters. One different group of nearby analogs are "Green Pea" galaxies, selected by their high equivalent width optical emission lines. Here we show that Green Pea galaxies have strong Ly α emission lines and high Ly α escape fraction (see also Henry et al. 2015), providing an opportunity to solve Ly α escape problem. Green Peas have a Ly α equivalent width distribution similar to high redshift Ly α emitters. The Ly α escape fraction correlates with many quantities of Ly α profile, especially the ratio of Ly α blue peak velocity to H α line width. Comparing Ly α profiles with expanding-shell radiative transfer models suggest these correlations are probably caused by column density and kinematics of neutral gas. The Ly α escape fraction also correlates with galactic metallicity and dust extinction. Studying Ly α in Green Peas can reveal how these various factors combine to make Ly α escape.

1. Introduction

The Ly α emission line is a key tool to discover high redshift galaxies and probe reionization. High redshift Ly α emission line galaxies (LAE) have been found routinely for almost two decades (e.g. Dey et al. 1998; Hu et al. 1998; Rhoads et al. 2000; Ouchi et al. 2003; Gawiser et al. 2006; Guaita et al. 2010; Clément et al. 2012; Shibuya et al. 2012;

Matthee et al. 2014). These high redshift LAEs generally are small young star forming galaxies. They have compact size, low stellar mass, low dust extinction, low metallicity, and high specific star formation rate (sSFR) (e.g. Bond et al. 2010; Malhotra 2012; Gawiser et al. 2007; Pirzkal et al. 2007; Finkelstein et al. 2008; Pentericci et al. 2009). They probably resemble the faint galaxies that dominate the the luminosity density of the universe in the epoch of reionization. At $2 \lesssim z \lesssim 6$, these LAEs are an important population of star-forming galaxies, and they constitute an increasing fraction of Lyman break galaxies across that range, reaching $\sim 60\%$ of Lyman break galaxies (LBGs) at redshift $z \sim 6$ (Stark et al. 2011). At $z > 6$, the $\text{Ly}\alpha$ luminosity, $\text{Ly}\alpha$ equivalent width (EW), and spatial clustering of LAEs and LBGs are used to probe reionization of intergalactic medium (e.g. Malhotra & Rhoads 2004; Ouchi et al. 2010; Hu et al. 2010; Kashikawa et al. 2011; Ota et al. 2010; Treu et al. 2012; Pentericci et al. 2014; Tilvi et al. 2014).

$\text{Ly}\alpha$ is a resonance line. Interactions between $\text{Ly}\alpha$ and neutral gas and dust are therefore complex. For the intrinsic $\text{Ly}\alpha$ photons generated from star formation, only a fraction can escape the galaxy and be observed (e.g. Charlot & Fall 1993; Ahn et al. 2001; Verhamme et al. 2006; Dijkstra et al. 2006). Thus to use $\text{Ly}\alpha$ as a tool to probe reionization, we should ideally understand how $\text{Ly}\alpha$ escapes from galaxies, which requires us to know galactic physical properties besides $\text{Ly}\alpha$ emission lines. While the high z LAEs are faint, we can only take relatively low resolution $\text{Ly}\alpha$ spectra and broad-band photometric measurements for most of them (e.g. Kashikawa et al. 2011). It is challenging to take rest frame optical spectra or other multi-band observations of these high- z LAEs (McLinden et al. 2011; Nakajima et al. 2013; Erb et al. 2014; Hashimoto et al. 2015). Due to difficulties of understanding $\text{Ly}\alpha$ escape in high- z LAEs, many studies turned to solve $\text{Ly}\alpha$ escape problem in nearby universe by observing galaxies with similar properties to high- z LAEs (e.g. Giavalisco et al. 1996; Kunth et al. 1998; Mas-Hesse et al. 2003; Deharveng et al. 2008; Atek et al. 2009, 2014; Scarlata et al. 2009; Leitherer et al. 2011; Heckman et al.

2011; Cowie et al. 2011; Wofford et al. 2013; Hayes et al. 2005, 2014; Ostlin et al. 2009, 2014; Pardy et al. 2014; Rivera-Thorsen et al. 2015). Most nearby star forming galaxies do not show Ly α emission or only have very weak Ly α emission lines (Cowie et al. 2010). Overall, the present sample of nearby Ly α emission line galaxies have on average much smaller Ly α equivalent width (EW(Ly α)) and Ly α escape fraction (1%-12% in Wofford et al. 2013 sample; Hayes et al. 2014) than do high- z LAE samples (>17% Zheng et al. 2012; Nakajima et al. 2012). The main exception is the recent Green Pea galaxy sample (Henry et al. 2015).

Green pea galaxies were discovered in the citizen project Galaxy Zoo, in which public volunteers morphologically classified millions of galaxies from the Sloan Digital Sky Survey (SDSS). These are compact galaxies so they appear round in SDSS images. The green color is because the [OIII] doublet dominates the light. They have redshifts $0.112 < z < 0.360$, small stellar masses $\sim 10^{8.5} - 10^{10.5} M_{sun}$, low metallicities, high specific star formation rates (sSFR), and emission line equivalent widths (EW(H α) and EW([OIII] λ 5007) exceeding hundreds of Å (Cardamone et al. 2009; Izotov et al. 2011). Thus Green Peas are good counterparts to high-redshift LAEs in size, morphology, stellar mass, metallicities, and optical emission line strengths. This suggested that Green Peas might also show strong Ly α emission lines.

Indeed observations of Green Peas showed strong Ly α emission lines (Jaskot et al. 2014, Henry et al. 2015). Nine of 12 Green Peas have EW(Ly α) > 30 Å. A lot of multi-wavelength studies of Green Peas are already in archive, and new observations are accessible. So Green Peas galaxies are a good opportunity to study Ly α escape. In this paper, we study Ly α spectra of a sample of archived Green Peas.

2. Green Peas Sample and Spectra Data

Green Peas were discovered by their green appearance in the Galaxy Zoo’s false-color *gri*-band images based on SDSS data. Since the *r* band was mapped to the green channel in these images, Green Peas correspond to objects where the SDSS *r*-band flux is dominated by line emission. While the full SDSS data set contains a few tens of thousands of Green Peas, they are not in a category systematically targeted for spectroscopic followup, and only a much smaller sample of about 251 Green Peas have spectra in SDSS DR7 (Cardamone et al. 2009). Further, to study galactic properties such as SFR, stellar mass, and metallicity, the spectra must have good signal to noise ratio (S/N) in both continuum and strong emission lines ($H\alpha$, $H\beta$, $[OIII]\lambda 5007$); and also have well-detected $[OIII]\lambda 4363$ emission lines. Galaxies with an active galaxies nucleus (AGN) (diagnosed by their broad Balmer emission lines or $H\alpha/[NII]$ vs. $[OIII]/H\beta$ diagram) are excluded. These selections result in 66 Green Peas that have good optical spectra and measured galactic properties (see Cardamone et al. 2009 and Izotov et al. 2011 for details about selection of Green Peas sample). Thus we have a parent Green Peas sample to investigate their $Ly\alpha$ emission properties.

We searched for UV spectra of these 66 Green Peas in the HST archive and find 12 Green Peas that have UV and $Ly\alpha$ spectra taken with the Cosmic Origins Spectrograph (COS) (PIs: Henry (GO: 12928); Jaskot (GO: 13293); Heckman (GO: 11727)). We study this sample of 12 Green Peas in this paper. The 9 galaxies in Henry’s sample were selected from the parent sample of 66 Green Peas by their FUV brightness, with $m_{FUV} < 20$ (*AB*). The 2 galaxies in Jaskot’s sample were selected by their extreme $[OIII]/[OII]$ ratios larger than 9. The one galaxy in Heckman’s sample was selected by its high FUV luminosity, high UV flux, and compact size. Comparing to the distribution of properties of the parent sample, these 12 peas are biased to higher UV brightness, higher SFR, lower stellar

mass, higher $\text{EW}([\text{OIII}])$, lower metallicity, and lower dust extinction. Figure 1 shows the metallicity and dust extinction ($\text{H}\alpha/\text{H}\beta$ ratio) of these 12 Green Peas compared to the parent sample.

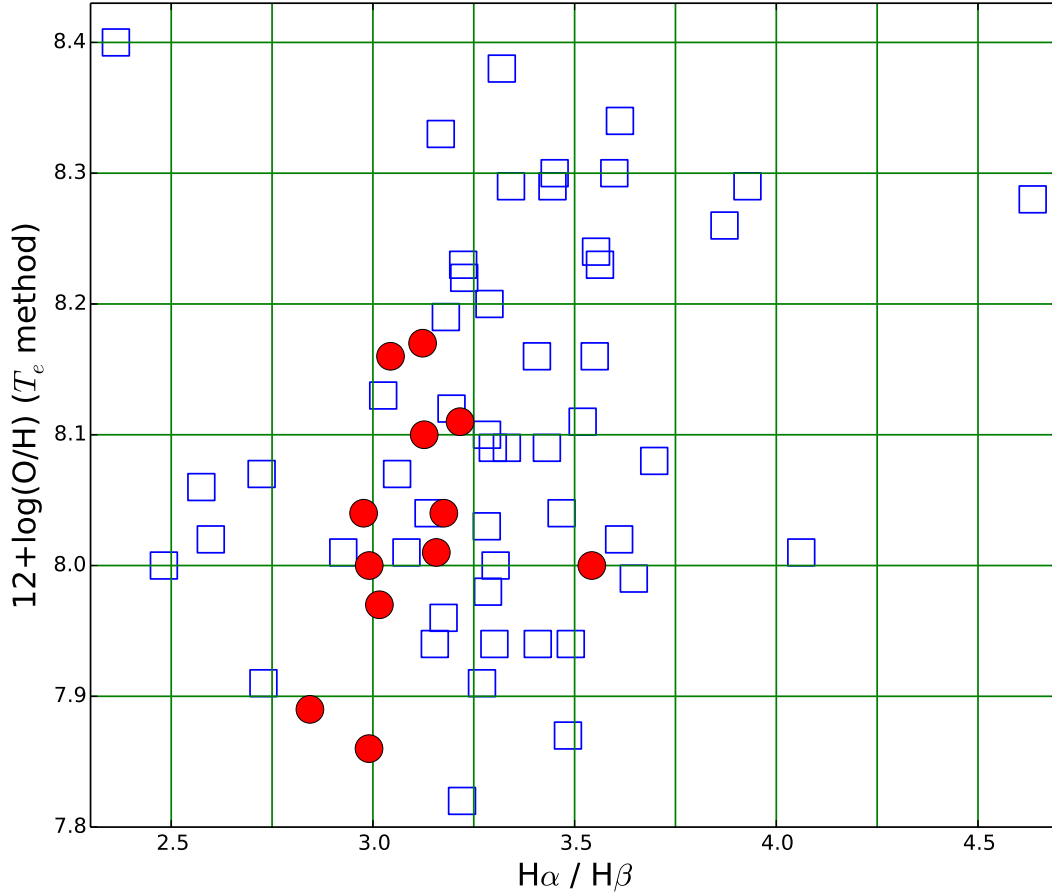


Fig. 1.— Green Peas sample distribution in the diagram of $\text{H}\alpha/\text{H}\beta$ and metallicity. $\text{H}\alpha/\text{H}\beta$ is measured flux ratio of $\text{H}\alpha$ and $\text{H}\beta$ emission lines. Red dots are the 12 Green Peas with $\text{Ly}\alpha$ spectra. Blue empty squares are the Green Peas of the parent sample.

All 12 Green Peas were imaged using the COS acquisition modes ACS/IMAGE, which took high resolution NUV acquisition images and centered the target accurately (error \sim

0.05 arc-second) in the 2.5 arc-seconds diameter Primary Science Aperture. These images show the NUV sizes of Green Peas are compact compared to the 2.5 arc-seconds aperture. Then FUV spectra were taken at four FP-POS settings. Rest-frame spectral coverages are $\sim 950\text{-}1500\text{\AA}$. $\text{Ly}\alpha$ spectra were taken with both FUV grating G130M and G160M for two sources. Since the $\text{Ly}\alpha$ were detected at very high S/N ratio, we only use G160M spectra for these two sources. 9 sources have $\text{Ly}\alpha$ spectra taken only with G160M. One source has $\text{Ly}\alpha$ spectra taken only with G130M.

We retrieved COS spectra for these 12 Green Peas from HST MAST archive after they have been processed through the standard COS pipeline CALCOS version 3.0 (2014-10-30). The resulting spectral resolutions are coarser than the spectra resolution $\text{FWHM} \sim 20 \text{ km s}^{-1}$ for point source, as these Green Peas are resolved in their NUV acquisition images. Their real spectral resolution depends on source angular sizes. For FUV continuum the resolutions are about $20\text{-}50 \text{ km s}^{-1}$ based on their NUV sizes (Henry et al. 2015; James et al. 2014). For $\text{Ly}\alpha$ emission line spectra, the resolution may be somewhat worse if $\text{Ly}\alpha$ is more extended than the UV continuum emission. If $\text{Ly}\alpha$ filled the aperture uniformly, the spectral resolution would be $\sim 200 \text{ km s}^{-1}$ FWHM (France et al. 2009). We also note that the COS spectroscopic line-spread function has extended wings broader than a Gaussian. We bin the reduced COS spectra to $\sim 0.12 \text{\AA pixel}^{-1}$ for 11 spectra taken with G160M and to $\sim 0.8 \text{\AA pixel}^{-1}$ for the one spectra taken with G130M. The velocity precisions of the UV spectra are better than 40 km s^{-1} (Henry et al. 2015). The precisions of the systemic redshifts from $\text{H}\alpha$ emission lines in SDSS spectra are better than 20 km s^{-1} . The resulting $\text{Ly}\alpha$ line profiles are shown in figure 2.

Then we measure the properties of $\text{Ly}\alpha$ emission lines. In most cases, we estimate the continuum level from rest-frame wavelength range $\sim 1225\text{-}1260 \text{\AA}$. For GP01 (see Table 1 for the source ID), the $\text{Ly}\alpha$ spectrum shows damped absorption wings, and we

measure the continuum from rest-frame wavelength range $\sim 1270\text{-}1300\text{\AA}$. For GP08, we don't have spectra red-ward of $\text{Ly}\alpha$, so we measure the continuum from rest-frame wavelength range $\sim 1180\text{-}1210\text{\AA}$. To get the $\text{Ly}\alpha$ line flux, we integrate the continuum subtracted spectra in rest-frame wavelength range $\sim 1210\text{-}1220\text{\AA}$. For GP01 with damped absorption, we get its residual $\text{Ly}\alpha$ emission line flux in the center of damped absorption without subtracting the continuum. We correct for Milky Way extinction using the attenuation measured by Schlafly & Finkbeiner (2011) and the Fitzpatrick (1999) extinction law. The foreground extinction values were obtained from the NASA/IPAC Galactic Dust Reddening and Extinction tool. Then we calculate the rest-frame $\text{EW}(\text{Ly}\alpha)$, $\text{EW}(\text{Ly}\alpha) = \text{Flux}(\text{Ly}\alpha) / f_{\lambda}(\text{continuum}) / (1 + \text{redshift})$.

We downloaded optical spectra of these Green Peas from the SDSS DR12 archive, along with the pipeline measurements of their emission line properties. We correct the measured $\text{H}\alpha$ and $\text{H}\beta$ fluxes for Milky Way extinction (again using the Fitzpatrick (1999) extinction law). Then we calculate $E(B-V)$ from dust in Green Peas galaxies using Calzetti et al. (2000) extinction law and an intrinsic $\text{H}\alpha/\text{H}\beta$ ratio of 2.86, and correct dust reddening of the observed $\text{H}\alpha$ flux. We use the metallicities and mass measured from SDSS spectra by Izotov et al. 2011. The metallicities were calculated using T_e method. These properties of Green Pea galaxies and their $\text{Ly}\alpha$ emission lines are shown in Table 1.

3. Green Peas as Analogs of High-z LAEs

The first remarkable result is all 12 Green Peas show $\text{Ly}\alpha$ emission lines (figure 2, see also Henry et al. (2015) for 10 of these 12 Green Peas). This is a much higher $\text{Ly}\alpha$ emission fraction than other nearby star-forming samples. Henry et al. (2015) compared Green Peas to two nearby $\text{Ly}\alpha$ samples – the LARS sample (Ostlin et al. 2014, Hayes et al. 2014), and the GALEX $z=0.3$ sample (Deharveng et al 2008; Finkelstein et al 2009; Cowie et al. 2011).

Table 1. Sample

ID	RA	DEC	$E(B - V)_{MW}$	Redshift	Ly α flux	EW(Ly α)	$f_{esc}^{Ly\alpha}$	V(blue-peak)	FWHM(H α)	12+log(O/H)	E(B-V)
	J2000	J2000	mag		$10^{-14} \text{ erg/s/cm}^2$	Å		km/s	km/s		mag
(1)	(2)	(3)	(4)	(5)	(6)	(7)	(8)	(9)	(10)	(11)	(12)
GP01	14:57:35.13	+22:32:01.79	0.0410	0.148611	0.46	7.36	0.014	-329	188	8.04	0.061
GP02	03:03:21.41	-07:59:23.2	0.0845	0.164880	1.01	7.20	0.050	-313	233	7.86	0.000
GP03	12:44:23.37	+02:15:40.4	0.0211	0.239426	1.89	39.96	0.065	-240	233	8.17	0.062
GP04	10:53:30.83	+52:37:52.9	0.0126	0.252638	1.54	10.66	0.068	-266	291	8.10	0.069
GP05	11:37:22.14	+35:24:26.7	0.0156	0.194390	3.81	33.43	0.130	-355	287	8.16	0.043
GP06	09:11:13.34	+18:31:08.2	0.0243	0.262200	3.15	49.53	0.155	-278	298	8.00	0.168
GP07	09:26:0.44	+44:27:36.54	0.0156	0.180690	6.36	40.82	0.245	-223	280	8.01	0.074
GP08	14:24:05.73	+42:16:46.3	0.0087	0.184788	8.55	78.27	0.266	-150	259	8.04	0.028
GP09	08:15:52.00	+21:56:23.65	0.0352	0.140950	4.01	75.09	0.299	-121	193	8.00	0.014
GP10	11:33:03.80	+65:13:41.3	0.0093	0.241397	2.08	35.29	0.352	-69	197	7.97	0.040
GP11	12:48:34.64	+12:34:02.9	0.0256	0.263389	5.28	94.80	0.383	- ^a	209	8.11	0.084
GP12	12:19:03.98	+15:26:08.5	0.0224	0.195599	13.45	157.54	0.672	-76	244	7.89	0.000

Note. — Column Descriptions: (1) Object ID; (4) The Milky Way extinction $E(B - V)_{MW}$ are measured by Schlafly & Finkbeiner (2011); (6) measured Ly α flux from the spectra. Ly α flux were corrected for Milky Way dust extinction using the Fitzpatrick (1999) extinction law. (7) rest-frame Ly α equivalent width; (8) Ly α escape fraction; (9) V(blue peak) is the velocity of the peak in the blue side of Ly α profile; (10) FWHM of H α emission line from SDSS spectra. (11) metallicity measured from direct T_e method by Izotov et al. 2011; (12) Dust extinction of Green Pea galaxies. Errors of these measurements are dominated by systematics, so statistical errors are not given.

^aGP#11 doesn't show double peak Ly α profile.

These Green Peas have on average smaller mass, higher UV luminosity, higher sSFR, higher $\text{EW}(\text{H}\alpha)$, lower dust extinction, and more compact size than the other two samples. Green Peas also have high $\text{EW}([\text{OIII}]\lambda 5007)$ and $[\text{OIII}]\lambda 5007/[\text{OII}]\lambda 3727$ ratio, which is similar to LAEs at redshift 2-3 (Mclinden et al. 2011; Nakajima et al. 2013). $\text{Ly}\alpha$ emission tends to be stronger in low mass, low dust extinction, and high $\text{EW}(\text{H}\alpha)$ galaxies (Cowie et al. 2011; Hayes et al. 2014; Atek et al. 2014). Many of these properties are correlated. Probably a combination of these properties explains the high $\text{Ly}\alpha$ detection fraction among the Green Peas.

9 of 12 Green Peas have $\text{EW}(\text{Ly}\alpha)$ larger than 30 \AA , and would be selected as LAEs in high redshift samples. We compare the $\text{EW}(\text{Ly}\alpha)$ distribution of Green Peas with other nearby and high- z LAE samples (figure 3). For the low- z comparison sample, we use GALEX grism-selected objects with $\text{EW}(\text{Ly}\alpha) \gtrsim 20 \text{ \AA}$ from both the Groth strip and NGPDWS fields (Cowie et al. 2011). We remove AGNs identified from optical spectra and multi-bands properties (Finkelstein et al. 2009, Scarlata et al. 2009). For the high z sample, we use $z=2.8$ narrow band selected LAEs sample in CDFS field (Zheng et al. 2015), and a combined sample of spectroscopically confirmed LAEs at $z=5.7$ and 6.5 (Kashikawa et al. 2011). All known AGNs in high z sample are excluded, and the AGN contamination for high z LAE sample is less than 5% (Zheng et al. 2013). The $\text{EW}(\text{Ly}\alpha)$ of high z samples are computed from narrow- and broad-band photometry. Most of the LAEs in both high z samples are detected in deep broad-band images, so the measured $\text{EW}(\text{Ly}\alpha)$ is accurate. For the Green Peas, GALEX LAE sample, and $z=2.8$ LAE sample, we calculate the accumulative normalized $\text{EW}(\text{Ly}\alpha)$ distribution by simply counting the observed $\text{EW}(\text{Ly}\alpha)$ of each sample. For the $z=5.7$ and 6.5 sample, the $\text{EW}(\text{Ly}\alpha)$ distribution was corrected for the faint sources incompleteness (Kashikawa et al. 2011). As shown in figure 3, the $\text{EW}(\text{Ly}\alpha)$ distribution of Green Peas is more similar to high redshift sample than to the GALEX $z=0.3$ LAE sample. According to K-S test results, the $\text{EW}(\text{Ly}\alpha)$ distribution of

GALEX LAE sample is different from that of $z=2.8$ LAE sample at a probability of 99%, while we can not distinguish the $EW(Ly\alpha)$ distribution of Green Peas sample from that of $z=2.8$ LAE sample (there is 57% probability that these two samples are different). So these Green Peas are not only similar to high z LAEs in many galactic properties like size, mass, and metallicities, they also have similar $Ly\alpha$ emission lines. Thus Green Peas are good local analogs of high- z LAEs.

4. $Ly\alpha$ Escape and $Ly\alpha$ Profiles

We now use Green Peas as a laboratory to study the mechanisms of $Ly\alpha$ escape. For these nearby galaxies, many galactic properties are well measured from UV and optical spectra, and we investigate how these properties relate to $Ly\alpha$ escape.

The $Ly\alpha$ escape fraction $f_{esc}^{Ly\alpha}$ is defined as the ratio of observed $Ly\alpha$ flux to intrinsic $Ly\alpha$ flux. Assuming case-B recombination, the intrinsic $Ly\alpha$ flux is 8.7 times dust extinction corrected $H\alpha$ flux. Thus the $f_{esc}^{Ly\alpha}$ is $Ly\alpha/(8.7 \times H\alpha_{corrected})$. The SDSS $H\alpha$ spectra were taken with 3 arc-seconds diameter aperture which is larger than the optical sizes of Green Peas, so the $H\alpha$ flux is the total flux of Green Pea galaxy. While $Ly\alpha$ may have more extended sizes than the COS 2.5 arc-seconds diameter aperture (Hayes et al. 2014), in that case using the observed $Ly\alpha$ flux underestimates the $Ly\alpha$ flux of the total Green Pea galaxy. So the $f_{esc}^{Ly\alpha}$ used here are smaller than the real $f_{esc}^{Ly\alpha}$ by an unknown aperture correction factor. For three Green Peas with total $Ly\alpha$ flux measured by GALEX grism observation or HST $Ly\alpha$ imaging, the COS aperture captured 40%-75% of the total $Ly\alpha$ flux (Henry et al. 2015).

The escape of the resonantly scattered $Ly\alpha$ photons involves potentially complex interactions with gas and dust. This results in richly varied $Ly\alpha$ line profiles that carry a

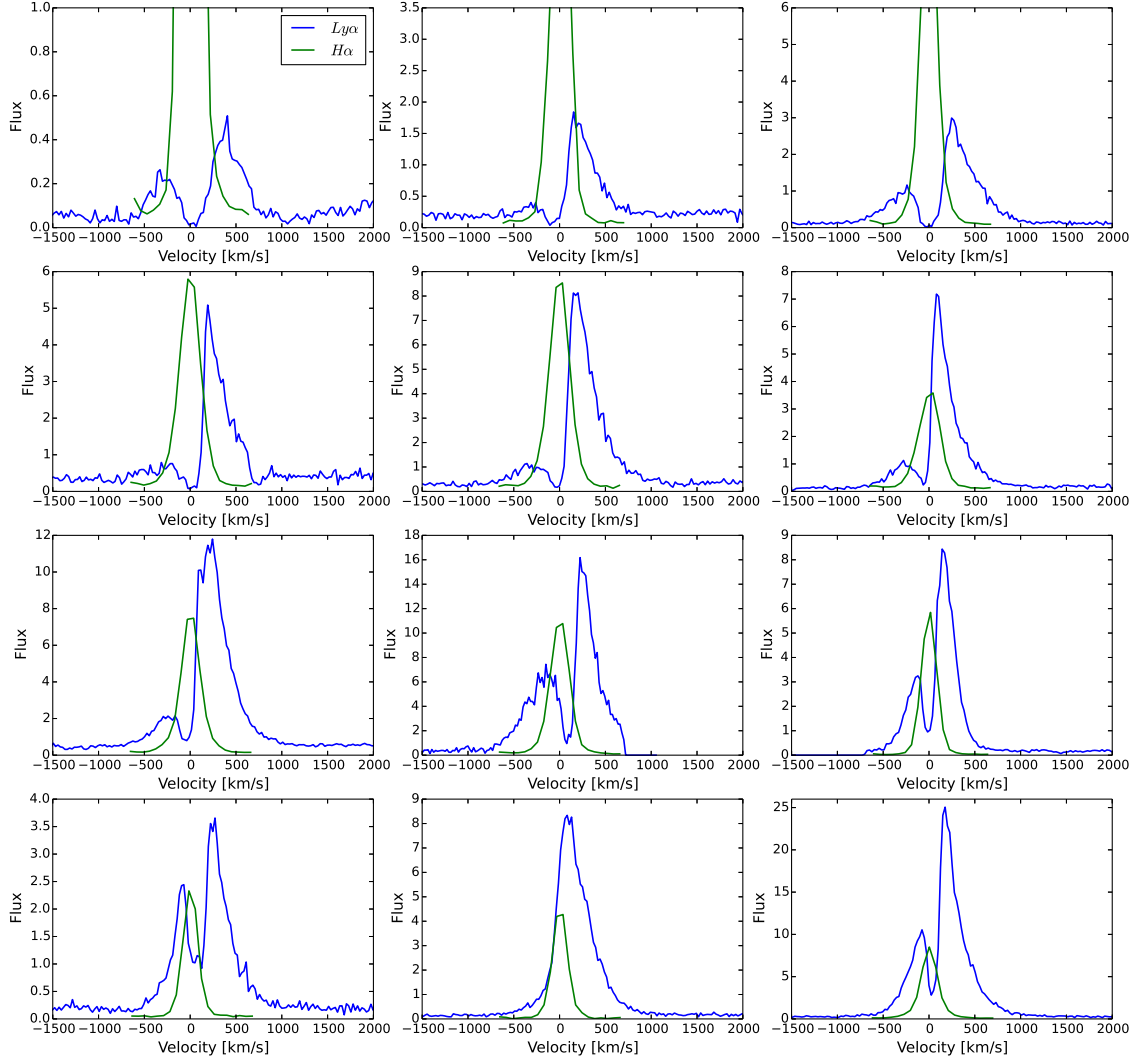


Fig. 2.— $\text{Ly}\alpha$ and $\text{H}\alpha$ emission line profiles of Green Peas. $\text{Ly}\alpha$ and $\text{H}\alpha$ are in the same flux units of $10^{-17} \text{erg cm}^{-2} \text{s}^{-1} (\text{km s}^{-1})^{-1}$ for all plots. These 12 galaxies are sorted by increasing $f_{\text{esc}}^{\text{Ly}\alpha}$ from left to right, and top to bottom. It shows that the $\text{Ly}\alpha$ profile evolves with $f_{\text{esc}}^{\text{Ly}\alpha}$ (see also Henry et al. (2015)).

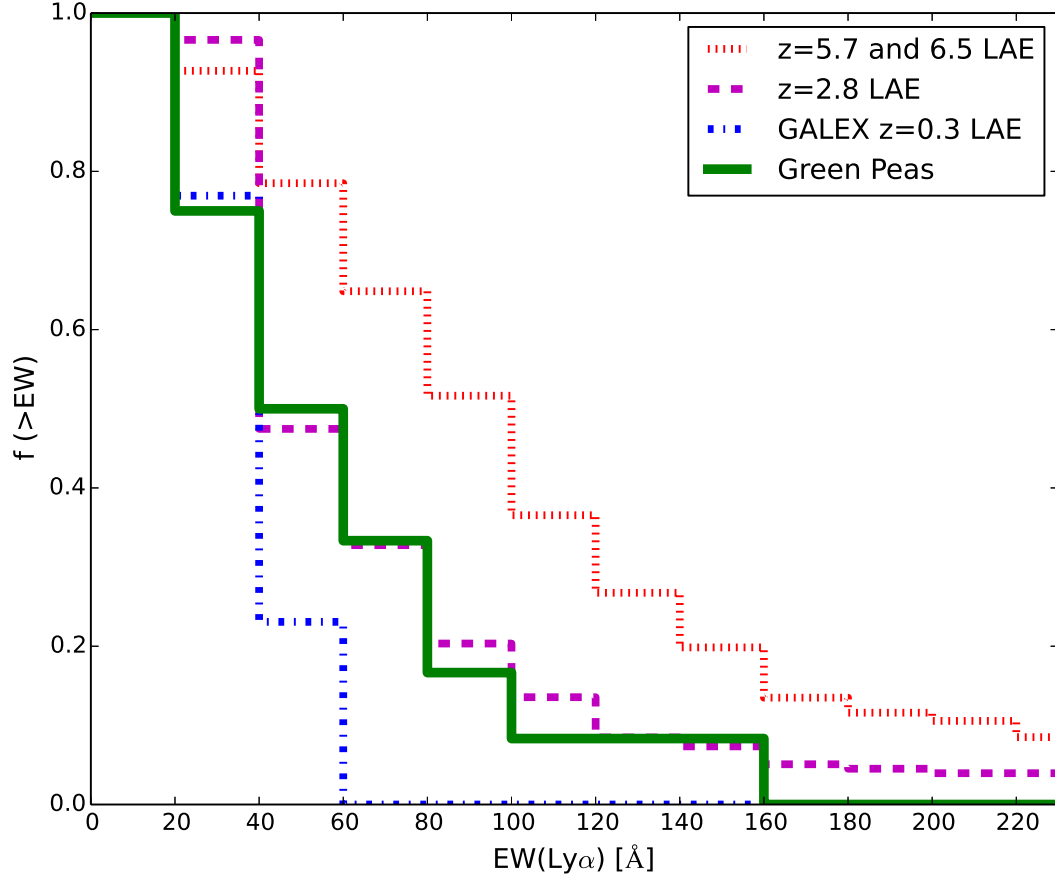


Fig. 3.— Comparing rest-frame $\text{EW}(\text{Ly}\alpha)$ distribution of Green Peas with different samples. Solid green line shows the 12 Green Peas. Dash-dot blue line shows the GALEX $z=0.3$ LAE sample from Cowie et al. (2011). Dashed magenta line shows the $z=2.8$ LAE sample from Zheng et al. (2015). Dotted red line shows the $z=5.7$ and 6.5 LAE sample from Kashikawa et al. (2011). The $\text{EW}(\text{Ly}\alpha)$ distribution of Green Peas is similar to the $z=2.8$ LAE sample.

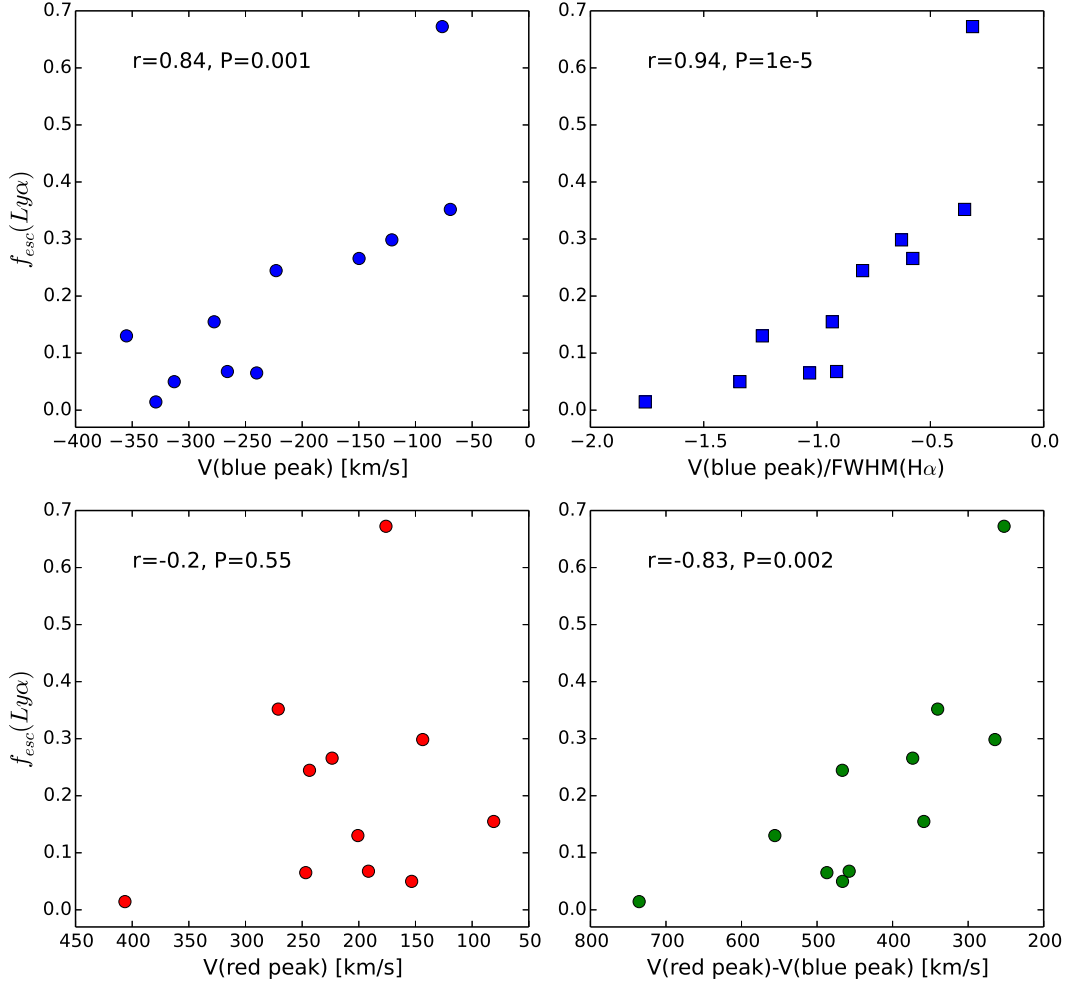


Fig. 4.— Relations between $f_{esc}^{Ly\alpha}$ and velocity quantities of Ly α profile. (Upper-left): $f_{esc}^{Ly\alpha}$ and velocity of blue peak of Ly α profile. (Upper-right): $f_{esc}^{Ly\alpha}$ and velocity of blue peak normalized by $\text{FWHM}(\text{H}\alpha)$. (Lower-left): $f_{esc}^{Ly\alpha}$ and velocity of red peak of Ly α profile. (Lower-right): $f_{esc}^{Ly\alpha}$ and peak separation of Ly α profile. The Spearman correlation coefficient r , and null probability P , are given in each panel.

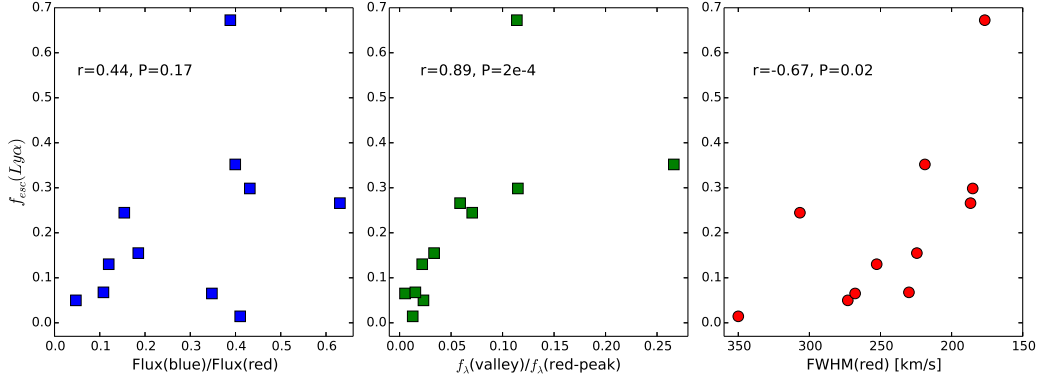


Fig. 5.— (Left): Relations between $f_{esc}^{Ly\alpha}$ and flux ratios of blue to red part of $Ly\alpha$ profile. (Middle): $f_{esc}^{Ly\alpha}$ and flux density ratio of valley to red peak of $Ly\alpha$ profile. (Right) $f_{esc}^{Ly\alpha}$ and FWHM of red part of $Ly\alpha$ profile. The Spearman correlation coefficient r , and null probability P , are given in each panel.

great deal of information, especially when the profiles are double-peaked as they tend to be for the Green Peas. We therefore begin by exploring relations between $f_{esc}^{Ly\alpha}$ and $Ly\alpha$ profiles.

In figure 2, we display the $Ly\alpha$ profiles of these 12 Green Peas in order of increasing $Ly\alpha$ escape fraction from left to right, and top to bottom. 11 have double-peaked line profiles. For these, we define the “red peak” as the peak in the $Ly\alpha$ line profile occurring at velocity > 0 . We similarly define the “blue peak” as the $Ly\alpha$ peak at velocity < 0 , and the “valley” as the flux minimum between the two peaks for double peak profiles. Simply looking at their profiles, we can find that as $f_{esc}^{Ly\alpha}$ increases, the residual flux at the inter-peak valley gets stronger, and the blue peak moves nearer to the systemic velocity (see also Henry et al. 2015). To characterize those trends quantitatively, we measure the velocity and flux density f_{λ} at the red peak, blue peak, and valley. We also measure the integrated flux and full width at half maximum (FWHM) for the red ($V > 0$) and blue ($V < 0$) portions of the $Ly\alpha$ profile – Flux(red), Flux(blue), FWHM(red), and FWHM(blue). Then

we investigate correlations between those quantities and Ly α escape fraction.

As shown in figure 4, $f_{esc}^{Ly\alpha}$ strongly correlates with the blue peak velocity V(blue-peak) (see also Henry et al. 2015) for the 11 Green Peas with double peaked profiles. The Spearman rank coefficient for this correlation is $r=0.84$ with a null probability of $P=0.001$.

As the gas that absorbs/scatters Ly α may have a distribution similar to the HII regions in the emitting galaxy, we normalize the blue peak velocity by the FWHM of H α . The $f_{esc}^{Ly\alpha}$ shows an even tighter correlation with the ratio V(blue-peak)/FWHM(H α), with Spearman rank coefficient $r=0.94$ and null probability $P=1e-5$. The $f_{esc}^{Ly\alpha}$ doesn't correlate with the red peak velocity (Spearman $r=-0.2$, $P=0.56$) or the ratio V(red-peak)/FWHM(H α) (Spearman $r=0.04$, $P=0.9$), while it does correlate with the peak separation V(red-peak)-V(blue-peak) (Spearman $r=-0.83$ and $P=0.002$) and (V(red-peak)-V(blue-peak))/FWHM(H α) (Spearman $r=-0.75$ and $P=0.007$). Thus correlations of $f_{esc}^{Ly\alpha}$ with velocity differences V(red-peak)-V(blue-peak) are mostly due to the stronger correlation with blue peak velocity. We also notice that in figure 2 Green Peas with large $f_{esc}^{Ly\alpha}$ (GP09, GP10, GP12) show V(Valley)>0, while the others with lower $f_{esc}^{Ly\alpha}$ have V(Valley)<0.

In figure 5, the $f_{esc}^{Ly\alpha}$ shows a very weak correlation with the flux ratio of blue and red part, Flux(blue)/Flux(red) (Spearman $r=0.44$, $P=0.17$). As the $f_{esc}^{Ly\alpha}$ increases, both the red and blue peak get stronger relative to the intrinsic Ly α flux. There is only a weak trend that the blue peak increases faster with $f_{esc}^{Ly\alpha}$ than the red peak. In the middle panel of figure 5, the $f_{esc}^{Ly\alpha}$ shows correlation with the residual flux $f_{\lambda}(valley)$ normalized by $f_{\lambda}(\text{red peak})$ (Spearman $r=0.89$ and $P=2e-4$). The $f_{\lambda}(\text{valley})/f_{\lambda}(\text{red peak})$ also correlates with V(blue peak) (Spearman $r=0.77$ and $P=0.005$) and V(blue peak)/FWHM(H α) (Spearman $r=0.80$ and $P=0.003$), because $f_{esc}^{Ly\alpha}$ correlates with both $f_{\lambda}(\text{valley})/f_{\lambda}(\text{red peak})$ and V(blue peak). In the right panel of figure 5, $f_{esc}^{Ly\alpha}$ shows correlation with FWHM(red) with Spearman $r=-0.67$ and $P=0.02$. It is not clear whether $f_{esc}^{Ly\alpha}$ also has weak correlation

with FWHM(blue), as the blue part profiles are noisy and the uncertainties of measured FWHM(blue) are too large. The $f_{esc}^{Ly\alpha}$ doesn't correlate with FWHM(H α) (Spearman $r=0.04$, $P=0.9$).

Although with 11 Green Peas we are suffering from small number statistics, these correlations are encouraging. We interpret these correlations between Ly α escape and Ly α profile in section 6.1.

5. Ly α Escape, Dust and Metallicities

We also investigate relations between $f_{esc}^{Ly\alpha}$ and galactic properties measured from optical spectra, namely the dust reddening E(B-V) and the metallicity. In the Ly α escape process, dust can absorb the Ly α photons and decrease $f_{esc}^{Ly\alpha}$. Multiple studies have confirmed that Ly α escapes more easily from galaxies with low dust reddening, and there is an anti-correlation between $f_{esc}^{Ly\alpha}$ and E(B-V), although dust extinction is not the only factor to determine $f_{esc}^{Ly\alpha}$ (Atek et al. 2008, 2014; Scarlata et al. 2009; Finkelstein et al. 2011; Cowie et al. 2011; Hayes et al. 2014). In the left panel of figure 6, we show the $f_{esc}^{Ly\alpha}$ - E(B-V) relation for Green Peas. It is qualitatively similar to previous studies, though this Green Peas sample has higher $f_{esc}^{Ly\alpha}$ and only covers a small E(B-V) range (see also figure 1). It is also consistent with the anti-correlation between EW(Ly α) and E(B-V) for high redshift galaxies (e.g. Shapley et al. 2003). There are two outliers in figure 6. One is GP02 (marked by a large circle) with the lowest metallicity and E(B-V). Its WISE three bands colors suggest it is the most probable AGN candidate in this sample (Malhotra et al, in preparation). The other one is GP11 (marked by a large square) which has single peaked line profile and large E(B-V). These two outliers confirmed that dust extinction is not the only factor to determine $f_{esc}^{Ly\alpha}$. After both GP02 and GP11 are excluded, the anti-correlation between $f_{esc}^{Ly\alpha}$ and E(B-V) has Spearman coefficient $r=-0.62$ and $P=0.05$. It

suggests dust extinction is still an important factor of Ly α escape even in this Green Peas sample covering a small E(B-V) range.

Dust reddening is usually higher in galaxies with higher metallicity and stellar mass. So we expect $f_{esc}^{Ly\alpha}$ may also correlate with metallicity. Some earlier studies find that Ly α escape is easier in low metallicity galaxies, while others find no correlation. Cowie et al. (2011) showed that GALEX selected z=0.3 LAE have metallicities systematically lower than UV-selected galaxies of similar continuum magnitude that show no Ly α emission. Finkelstein et al. (2011) also show that GALEX selected z=0.3 LAE have lower metallicities than similar-mass galaxies from the SDSS. While Atek et al. (2014) showed that there is no correlation between $f_{esc}^{Ly\alpha}$ and metallicity for a combined z=0-0.3 LAE sample. Hayes et al. (2014) showed that in the LARS sample with 14 LAEs, a few galaxies with high $f_{esc}^{Ly\alpha}$ have on average lower metallicity than the other few galaxies with low $f_{esc}^{Ly\alpha}$. We note that metallicity of the LARS galaxies are measured with spectra from a small region of galaxies, while $f_{esc}^{Ly\alpha}$ is measured for the total galaxies. Another problem of those studies are that the metallicities measured from the strong line index ([NII]/H α , ([OII]+[OIII])/H β , or ([OIII]/H β)/([NII]/H α) have large uncertainties.

For this Green Peas sample, we show the relations between $f_{esc}^{Ly\alpha}$ and metallicity measured from the more accurate T_e method using optical spectra of the total galaxy (right panel of figure 6). If both outliers GP02 and GP11 are excluded, $f_{esc}^{Ly\alpha}$ correlates with metallicity with Spearman coefficient r=-0.82 and P=0.004. As most of those Green Peas have $f_{esc}^{Ly\alpha}>0.1$, while most of galaxies in the sample of Atek et al. (2014) have $f_{esc}^{Ly\alpha}<0.1$, it may suggest that metallicity plays an important role in galaxies with high $f_{esc}^{Ly\alpha}$, like Green Peas and high redshift LAEs.

What causes the correlation of $f_{esc}^{Ly\alpha}$ and metallicity? If it is caused from a positive correlation between metal and dust abundance, then a tighter correlation between $f_{esc}^{Ly\alpha}$

and $E(B-V)$ would be expected. While the data shows that $f_{esc}^{Ly\alpha}$ - metallicity has tighter correlation. It suggests that metallicity influence $f_{esc}^{Ly\alpha}$ through factors other than dust. In low metallicity galaxies, the ionizing spectra are steeper and can ionize more HI gas, thus probably reducing the optical depth of $Ly\alpha$ and making $Ly\alpha$ escape easier.

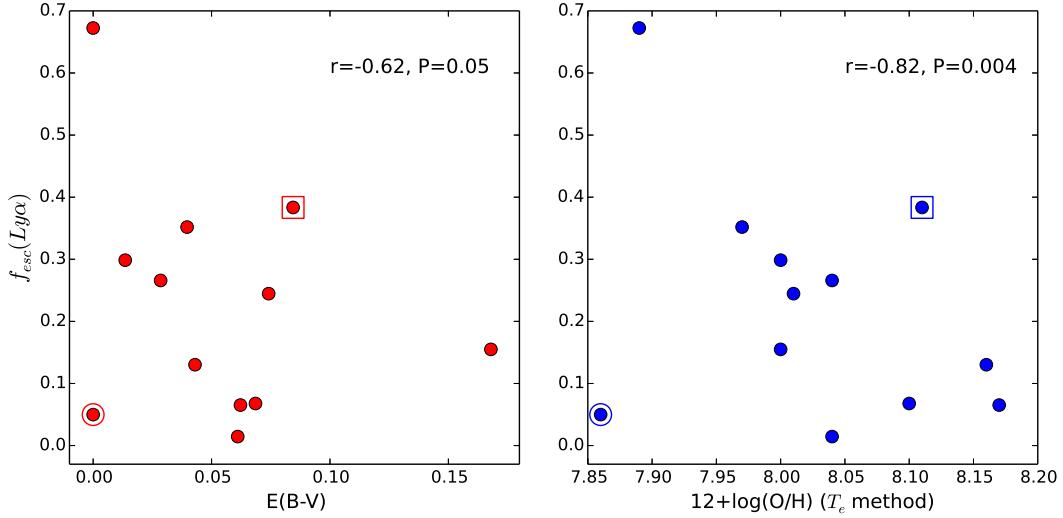


Fig. 6.— (Left): Relations between $f_{esc}^{Ly\alpha}$ and dust extinction $E(B-V)$. (Right): $f_{esc}^{Ly\alpha}$ and metallicity. The Spearman correlation coefficient r , and null probability P , are given in each panel. GP02 (marked by a large circle) has the lowest metallicity and $E(B-V)$. Its WISE three bands colors suggest it is probably an AGN (Malhotra et al. in-prep). GP11 (marked by a large square) has single peak profile and large $E(B-V)$. We exclude both sources when calculating correlation coefficients.

6. Discussion

6.1. Correlations between $f_{esc}^{Ly\alpha}$ and $Ly\alpha$ Profile

To understand correlations between $Ly\alpha$ escape and $Ly\alpha$ profile, we need to understand the complex $Ly\alpha$ radiative transfer process. As $Ly\alpha$ is a resonant line, the HI gas in a galaxy can have large optical depth for the $Ly\alpha$ photons near line center. The HI gas scatters and absorbs the $Ly\alpha$ photons near the line center and allows the escape of photons with large off-resonance velocity, thus generating double peaked profiles. Scattering of HI also increases the photons' path length within the galaxy, potentially increasing the effect of dust on the $Ly\alpha$ line. The measured quantities (velocity and f_λ) of the double peaked profile depend on the kinematics of the gas, HI column density (N_{HI}), gas temperature, and dust opacity. With this basic picture of $Ly\alpha$ radiative transfer process, we interpret the correlations between $f_{esc}^{Ly\alpha}$ and $Ly\alpha$ profile by comparing with radiative transfer models.

(1) $f_{esc}^{Ly\alpha}$, **V(blue peak)**, **V(red peak)**, and f_λ (**valley**): As shown in section 4, the $f_{esc}^{Ly\alpha}$ correlates strongly with V(blue peak) and peak separation, while the correlation with V(red peak) is not significant. As the red peak of $Ly\alpha$ is usually stronger and V(red peak) is easier to measure, the relation between V(red peak) and $Ly\alpha$ escape has been studied by many groups. EW($Ly\alpha$) anti-correlates with V(red peak) for redshift 2-3 galaxies (Erb et al. 2014, Shibuya et al. 2014, Hashimoto et al. 2015). The scatter of EW($Ly\alpha$)-V(red peak) relation is large if only considering galaxies with $0 < V(\text{red peak}) < 300 \text{ km s}^{-1}$. The Green Pea sample only covers this restricted V(red peak) range, so lack of correlation between $f_{esc}^{Ly\alpha}$ and V(red peak) remains consistent with the correlation seen for high- z LAE samples.

The EW($Ly\alpha$) and V(red peak) relation can be interpreted by two kinds of models. The first kind of model assumes there is a gas component with velocity distribution near systemic velocity and another outflowing gas component (e.g. Steidel et al. 2010). The gas

component near systemic velocity absorbs central part of Ly α profile and moves the red peak red-ward. Stronger absorption by this gas component will cause smaller EW(Ly α), larger V(red peak), and smaller f_λ (valley). The other kind of model assumes the gas is distributed in an expanding shell and Ly α profile is built through scattering with the gas shell (e.g. Ahn et al. 2001; Verhamme et al. 2006; Dijkstra et al. 2006; Schaerer et al. 2011). The expanding shell model also predicts that when N_{HI} and gas temperature are smaller, the Ly α escape is easier, and the V(red peak) and peak separation are larger (Verhamme et al. 2015).

While those models can explain the EW(Ly α) - V(red peak) relation, they don't explain why the V(red peak) doesn't correlate with EW(Ly α) and $f_{esc}^{Ly\alpha}$, but the V(blue peak) correlates with EW(Ly α) and $f_{esc}^{Ly\alpha}$. It seems that when $f_{esc}^{Ly\alpha}$ increases, the factors that help Ly α escape combine to decrease V(blue peak), while the effect of those factors on V(red peak) are canceled out.

To explore the physical origin of these trends, we fit the Ly α profiles of Green Peas with expanding shell radiative transfer models (Dijkstra et al. 2014; Gronke et al. 2015). The models give good fits for profiles of 9/12 Green Peas, but fail to fit well the three double peak profiles with highest $f_{esc}^{Ly\alpha}$ (GP12, GP10, GP09). The poor fit for those three Green Peas (GP12, GP10, GP09) is likely because they all show V(Valley)>0 (see section 4 and figure 2), which suggests absorption by *inflowing* gas. We will report fitting with improved models in a following paper. We plot $f_{esc}^{Ly\alpha}$ as a fraction of fitted N_{HI} in figure 7. For the 9 cases where the model fitting proceeded smoothly, the plotted N_{HI} is determined by full Markov Chain Monte Carlo fits (as described in Gronke et al 2015). For the remaining three cases, the plotted N_{HI} is determined by manually adjusting the model parameters to match the observed depth of the “valley” and heights of the blue and red peaks. The best fit results suggest an anti-correlation between $f_{esc}^{Ly\alpha}$ and N_{HI} with Spearman $r=-0.69$ and

$P=0.01$ (figure 7). Therefore we conclude that the low column density of neutral gas, N_{HI} plays an important role in the process of $Ly\alpha$ escape in these Green Peas.

(2) $f_{esc}^{Ly\alpha}$ and $V(\text{blue peak})/\text{FWHM}(H\alpha)$: What causes the strongest correlation between $f_{esc}^{Ly\alpha}$ and $V(\text{blue peak})/\text{FWHM}(H\alpha)$? If we assume there is a HI gas component with similar velocity distribution to that of the H II regions traced by $H\alpha$ emission, the correlation $f_{esc}^{Ly\alpha}$ - $V(\text{blue peak})/\text{FWHM}(H\alpha)$ may suggest that this HI gas component is important for $Ly\alpha$ escape. Another clue is that the $H\alpha$ emission lines of a few Green Peas in this sample show weak broad wings (also noted by Amorín et al. 2012, Jaskot & Oey 2014, and Henry et al. 2015). The broad wings likely trace outflowing ionized gas. As the $\text{FWHM}(H\alpha)$ used here are from fitting with single gaussian model, fitting a $H\alpha$ profile with a narrow core component and broad wings will result in larger best fit $\text{FWHM}(H\alpha)$ than only fitting the narrow core component. We note that two Green Peas with the most obvious broad $H\alpha$ wings (GP07, GP12) also show larger $f_{esc}^{Ly\alpha}$ than the $f_{esc}^{Ly\alpha}$ - $V(\text{blue peak})$ trend in figure 4. It suggests the outflowing ionized gas traced by broad $H\alpha$ wings can help $Ly\alpha$ escape.

(3) $f_{esc}^{Ly\alpha}$ and $\text{Flux}(\text{blue})/\text{Flux}(\text{red})$: The $f_{esc}^{Ly\alpha}$ shows very weak correlation with the flux ratio of blue and red part. This is consistent with the relation between $\text{Flux}(\text{blue})/\text{Flux}(\text{red})$ and $\text{EW}(Ly\alpha)$ for $z=2-3$ galaxies sample (Erb et al. 2014). Their rest-frame UV color-selected sample shows correlations between $\text{Flux}(\text{blue})/\text{Flux}(\text{red})$ and $\text{EW}(Ly\alpha)$, while LAE sample shows large scatter. The $\text{Flux}(\text{blue})/\text{Flux}(\text{red})$ ratio is mainly determined by the expanding velocity of outflowing gas (e.g. Verhamme et al. 2015). Increasing gas outflow velocity makes the blue peak weaker. 11/12 of Green Peas have double peaked profiles, and have stronger blue peaks than other nearby samples. This suggests the gas in Green Peas has a relatively small outflow velocity. Our best fit shell expansion velocities are smaller than 130 km s^{-1} for those 11 Green Peas with double peak

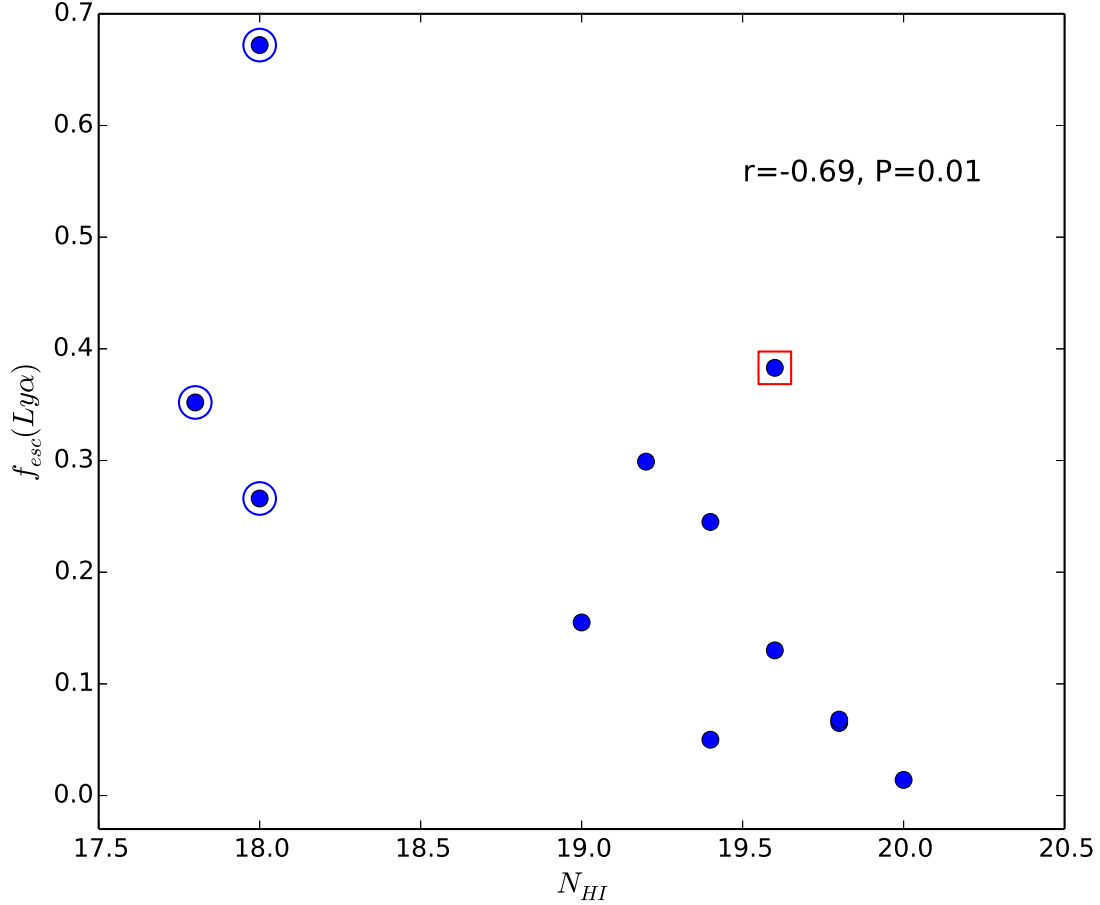


Fig. 7.— Relations between $f_{esc}^{Ly\alpha}$ and best fit N_{HI} from an expanding shell model (Gronke et al 2015). N_{HI} was derived by MCMC fitting of the shell model parameters except for GP07, GP03, and GP05 (marked by large circles), where the fitting procedure failed, most likely because the expanding shell models cannot reproduce the observed $V_{valley} > 0$. In these three cases, we plot the N_{HI} obtained by manually adjusting the model parameters to match the observed depth of the “valley” and the height of blue and red peaks, which should yield a moderately reliable N_{HI} . GP11 (marked by a large square) has single peak profile and large E(B-V). The Spearman correlation coefficient r , and null probability P , are calculated with all 12 sources. GP03 and GP04 have almost the same $f_{esc}^{Ly\alpha}$ and N_{HI} and overlap in this plot.

profiles, based on the shell model fitting discussed above. This result is in tension with the large gas outflow velocity (a few hundred km s^{-1}) inferred from low-ionization interstellar metal absorption lines (Henry et al. 2015).

(4) Ly α Line Width: The double peaked Ly α profiles of Green Peas have large peak separations ($\sim 250\text{--}750 \text{ km s}^{-1}$). As the intrinsic H α FWHM of Green Peas are about 200 km s^{-1} , to generate such large peak separations with an expanding shell model requires high N_{HI} and expansion velocity. However, the strong blue peak of Ly α profile and high $f_{\text{esc}}^{\text{Ly}\alpha}$ suggest low N_{HI} and expansion velocity. To solve the conflict, our model fitting results (discussed above) have intrinsic Ly α line widths that are $\sim 2\text{--}3$ times larger than the intrinsic H α width. Hashimoto et al. (2015) use expanding shell models to fit Ly α profiles of a few $z \sim 2$ LAEs with known nebular line widths (H α or [OIII] $\lambda 5007$). They also found the best fit intrinsic Ly α width is a few times larger than the intrinsic H α width. Ly α and H α powered by star formation ought to originate in the same gas, so a wider intrinsic Ly α profile would suggest either that not all the Ly α is powered by star formation (cf. Hashimoto et al 2015), or that there are important radiative transfer effects that broaden Ly α nearer to the source, before it encounters the model’s expanding outer HI shell.

6.2. What Makes Ly α Emitters with High $f_{\text{esc}}^{\text{Ly}\alpha}$?

What makes a star-forming galaxy into a Ly α emitter with high $f_{\text{esc}}^{\text{Ly}\alpha}$? In a young star-forming galaxy, the ionizing photons from young massive stars generate a lot of Ly α photons. The Ly α photons’ escape is influenced by four main factors: 1) low column density of neutral gas; 2) scarcity of dust in low metallicity galaxies; 3) gas outflow which takes photons out of resonance; and 4) a small covering factor of clumpy dense gas. From the Green Peas, we learn that high $f_{\text{esc}}^{\text{Ly}\alpha}$ Ly α emitters have low HI column density, which is a dominant factor in the observed correlations between $f_{\text{esc}}^{\text{Ly}\alpha}$, $V(\text{blue peak})$ and $f_{\lambda}(\text{valley})$.

The $f_{esc}^{Ly\alpha}$ is also anti-correlated with dust extinction. The metallicity of Ly α emitters shows a strong anti-correlation with the escape fraction $f_{esc}^{Ly\alpha}$. All Green Peas have gas outflows with high outflowing velocity, based on low ionization interstellar lines (Henry et al 2015). Gas outflows are probably necessary for Ly α escape. However, the varied Ly α profiles suggest complex interactions between Ly α photons and gas kinematics, which is probably responsible for the lack of correlation between outflow velocity and $f_{esc}^{Ly\alpha}$. It is possible that many of these factors are correlated, and multiple factors can combine to produce high $f_{esc}^{Ly\alpha}$. For example, galaxies where the absorption column of neutral gas as well as metallicity is low will show higher $f_{esc}^{Ly\alpha}$. Kinematics of outflows that take Ly α photons out of resonance also help.

7. Conclusion

We show that all Green Peas show strong Ly α emission lines; 9/12 of them have $EW(Ly\alpha) > 30\text{\AA}$ and would be selected as LAE in high redshift sample. This sample of Green Peas have $EW(Ly\alpha)$ distribution similar to high redshift LAEs. The $f_{esc}^{Ly\alpha}$ of Green Peas correlate with many quantities of Ly α profile, especially the ratio $V(\text{blue peak})/FWHM(H\alpha)$. Comparing the Ly α profiles with expanding shell models suggest these correlations are probably caused by variations of N_{HI} and gas kinematics. The $f_{esc}^{Ly\alpha}$ also correlates with metallicity and dust extinction. Thus Green Peas are very good analogs of high redshift LAEs with high $f_{esc}^{Ly\alpha}$, and provide great labs to study Ly α escape. However, with the current 12 Green Pea galaxies, the above results are subjected to small number statistics and the relative importance of various factors - metallicity/dust vs kinematics are hard to determine. With UV spectral observations of a larger sample of Green Peas, we may be able to determine the relative individual role of various factors in how Ly α escapes.

We thank M. S. Oey for helpful discussions. H. Y. acknowledges support from China Scholarship Council.

REFERENCES

- Ahn, S.-H., Lee, H.-W., & Lee, H. M. 2001, *ApJ*, 554, 604
- Amorín, R., Grazian, A., Castellano, M., et al. 2014, *ApJ*, 788, L4
- Atek, H., Schaerer, D., & Kunth, D. 2009, *A&A*, 502, 791
- Atek, H., Kunth, D., Hayes, M., Östlin, G., & Mas-Hesse, J. M. 2008, *A&A*, 488, 491
- Atek, H., Kunth, D., Schaerer, D., et al. 2014, *A&A*, 561, A89
- Bond, N. A., Feldmeier, J. J., Matković, A., et al. 2010, *ApJ*, 716, L200
- Calzetti, D., Armus, L., Bohlin, R. C., et al. 2000, *ApJ*, 533, 682
- Cardamone, C., Schawinski, K., Sarzi, M., et al. 2009, *MNRAS*, 399, 1191
- Charlot, S., & Fall, S. M. 1993, *ApJ*, 415, 580
- Clément, B., Cuby, J.-G., Courbin, F., et al. 2012, *A&A*, 538, A66
- Cowie, L. L., Barger, A. J., & Hu, E. M. 2011, *ApJ*, 238, 136
- Deharveng, J.-M., Small, T., Barlow, T. A., et al. 2008, *ApJ*, 680, 1072
- Dey, A., Spinrad, H., Stern, D., Graham, J. R., & Chaffee, F. H. 1998, *ApJ*, 498, L93
- Dijkstra, M., Haiman, Z., & Spaans, M. 2006, *ApJ*, 649, 14
- Erb, D. K., Steidel, C. C., Trainor, R., et al. 2014 *ApJ*, 795, 33
- Finkelstein, S. L., Rhoads, J. E., Malhotra, S., Grogin, N., & Wang, J. 2008, *ApJ*, 678, 655
- Finkelstein, S. L., Cohen, S. H., Malhotra, S., et al. 2009, *ApJ*, 703, L162
- Finkelstein, S. L., Cohen, S. H., Moustakas, J., et al. 2011, *ApJ*, 733, 117

- Fitzpatrick, E. L. 1999, *PASP*, 111, 63
- France, K., Beasley, M., Keeney, B. A., et al. 2009, *ApJ*, 707, L27
- Gawiser, E., van Dokkum, P. G., Gronwall, C., et al. 2006, *ApJ*, 642, L13
- Gawiser, E., Francke, H., Lai, K., et al. 2007, *ApJ*, 671, 278
- Gialalisco, M., Koratkar, A., & Calzetti, D. 1996, *ApJ*, 466, 831
- Guaita, L., Gawiser, E., Padilla, N., et al. 2010, *ApJ*, 714, 255
- Hashimoto, T., Verhamme, A., Ouchi, M., et al. 2015, *arXiv:1504.03693*
- Hayes, M., Östlin, G., Mas-Hesse, J. M., et al. 2005, *A&A*, 438, 71
- Hayes, M., Östlin, G., Duval, F., et al. 2014, *ApJ*, 782, 6
- Heckman, T. M., Borthakur, S., Overzier, R., et al. 2011, *ApJ*, 730, 5
- Henry, A., Scarlata, C., Martin, C., & Erb, D. 2015, *arXiv:1505.05149*
- Hu, E. M., Cowie, L. L., & McMahon, R. G. 1998, *ApJ*, 502, L99
- Hu, E. M., Cowie, L. L., Barger, A. J., et al. 2010, *ApJ*, 725, 394
- Izotov, Y. I., Guseva, N. G., & Thuan, T. 2011, *ApJ*, 728, 161
- James, B. L., Aloisi, A., Heckman, T., Sohn, S. T., & Wolfe, M. A. 2014, *ApJ*, 795, 109
- Jaskot, A. E. & Oey, M. S. 2014, *ApJ*, 791, 19L
- Kashikawa, N., Shimasaku, K., Matsuda, Y., et al. 2011, *ApJ*, 734, 119
- Kunth, D., Mas-Hess, J. M., Terlevich, E., et al. 1998, *A&A*, 334, 11
- Leitherer, C., Tremonti, C. A., Heckman, T. M., & Calzetti, D. 2011, *AJ*, 141, 37

- Malhotra, S., & Rhoads, J. E. 2004, *ApJ*, 617, L5
- Malhotra, S., Rhoads, J. E., Finkelstein, S. L., et al. 2012, *ApJ*, 750, L36
- Mas-Hesse, J. M., Kunth, D., Tenorio-Tagle, G., et al. 2003, *ApJ*, 598, 858
- Matthee, J. J. A., Sobral, D., Swinbank, A. M., et al. 2014, *MNRAS*, 440, 2375
- McLinden, E. M., Finkelstein, S. L., Rhoads, J. E., et al. 2011, *ApJ*, 730, 136
- Nakajima, K., Ouchi, M., Shimasaku, K., et al. 2012, *ApJ*, 745, 12
- Nakajima, K., Ouchi, M., Shimasaku, K., et al. 2013, *ApJ*, 769, 3
- Östlin, G., Hayes, M., Kunth, D., et al. 2009, *AJ*, 138, 923
- Östlin, G., Hayes, M., Duval, F., et al. 2014, *ApJ*, 797, 11
- Ota, J., Iye, M., Kashikawa, N., et al. 2010, *ApJ*, 722, 803
- Ouchi, M., Shimasaku, K., Furusawa, H., et al. 2003, *ApJ*, 582, 60
- Ouchi, M., Shimasaku, K., Furusawa, H., et al. 2010, *ApJ*, 723, 869
- Pardy, S. A., Cannon, J. M., Östlin, G., et al. 2014, *ApJ*, 794, 101
- Pentericci, L., Grazian, A., Fontana, A., et al. 2009, *A&A*, 494, 553
- Pentericci, L., Vanzella, E., Fontana, A., et al. 2014, *ApJ*, 793, 113
- Pirzkal, N., Malhotra, S., Rhoads, J. E., & Xu, C. 2007, *ApJ*, 667, 49
- Rhoads, J. E., Malhotra, S., Dey, A., et al. 2000, *ApJ*, 545, L85
- Rivera-Thorsen, T. E., Hayes, M., Östlin, G., et al. 2015, *ApJ*, 805, 14
- Scarlata, C., Colbert, J., Teplitz, H. I., et al. 2009, *ApJ*, 705, 98L

- Schaerer, D., Hayes, M., Verhamme, A., & Teyssier, R. 2011, *A&A*, 531, A12
- Schlaafy, E. F. & Finkbeiner, D. F. 2011, *ApJ*, 737, 103
- Shapley, A. E., Steidel, C. C., Pettini, M., & Adelberger, K. L. 2003, *ApJ*, 588, 65
- Shibuya, T., Kashikawa, N., Ota, K., et al. 2012, *ApJ*, 752, 114
- Shibuya, T., Ouchi, M., Nakajima, K., et al. 2014, *ApJ*, 788, 74
- Stark, D. P., Ellis, R. S., & Ouchi, M. 2011, *ApJ*, 728, L2
- Steidel, C. C., Erb, D. K., Shapley, A. E., et al. 2010, *ApJ*, 717, 289
- Tilvi, V., Papovich, C., Finkelstein, S. L., et al. 2014, *ApJ*, 794, 5
- Treu, T., Trenti, M., Stiavelli, M., Auger, M. W., & Bradley, L. D. 2012, *ApJ*, 747, 27
- Verhamme, A., Schaerer, D., & Maselli, A. 2006, *A&A*, 460, 397
- Verhamme, A., Orlitová, I., Schaerer, D., & Hayes, M. 2015, *A&A*, 578, A7
- Wofford, A., Leitherer, C., & Salzer, J. 2013, *ApJ*, 765, 118
- Zheng, Z.-Y., Malhotra, S., Wang, J.-X., et al. 2012, *ApJ*, 746, 28
- Zheng, Z.-Y., Finkelstein, S. L., Finkelstein, K., et al. 2013, *MNRAS*, 431, 3589